

INTRODUCTION

Eutrophication is the state of having high nutrient content and high organic production (Wetzel, 1983) and many freshwater systems in the world are affected by it. Eutrophication diminishes water quality by promoting the excessive growth of algae, cyanobacteria (blue-green algae) and macrophytes. Environmental researchers have been making efforts to monitor, simulate and control eutrophication for more than two decades. Various mathematical models have been developed and applied to rivers, lakes and estuaries (e.g. Lung, 1986; Thomann and Mueller, 1987; Kuo and Wu, 1991; Kuo et al., 1994). Most water quality models simulate increases in eutrophication based on initial conditions of the water body, therefore, demanding comprehensive water quality sampling programs. However, the conventional measurement of water quality requires in situ sampling and expensive and time-consuming laboratory work. Due to these limitations, the sample size often cannot be large enough to cover the entire water body. Therefore, the difficulty of synoptic and successive water quality sampling becomes a barrier to water quality monitoring and forecasting.

Remote sensing could overcome these constraints by providing an alternative means of water quality monitoring over a range of temporal and spatial scales. A number of studies have shown that applications of remote sensing can meet the demand for the large sample sizes required of water quality studies conducted on the watershed scale. Imagery from satellite and aircraft remote sensing systems has been used in the assessment of water quality parameters such as temperature, chlorophyll *a*, turbidity, and total suspended solids (TSS) for lakes and reservoirs (Lillesand et al., 1983; Lathrop and Lillesand, 1989; Ritchie and Cooper, 1991), estuaries (Verdin, 1985; Harding et al., 1995) and tropical coastal areas (Ruiz-Azuara, 1995).

Previous studies have focused on the discovery of the relationship between remote sensing data and in-situ measurements. To make remote sensing tools useful for practical applications, water quality modeling must be incorporated with water quality monitoring programs. Moreover, integrating a geographic information system (GIS) data allows for the display of refined monitoring simulation results, rather than the use of traditional numerical figures. This provides a means by which water quality modeling data can be presented in a way that is practical for water quality management. The specific objectives of this study were to: 1) establish a model to process remote sensing data and provide a rapid and efficient water quality monitoring technique for a wide area, 2) present predicted water quality conditions temporally and spatially on a georeferenced map and 3) display sequential (temporal) images of water quality predictions to provide decision makers with easily understandable information.

Turbidity

Turbidity is a unit of measurement quantifying the degree to which light traveling through a water column is scattered by the suspended organic (including algae) and inorganic particles. The scattering of light increases with a greater suspended load. Turbidity is commonly measured

in Nephelometric Turbidity Units (NTU). The acceptable NTU ranges for turbidity are given in Table 1.

Table 1: Acceptable NTU ranges for turbidity.

Designated Use	Acceptable Ranges (NTU)	Reference
Aquatic Life	< 50 (instantaneous)	Harvey, 1989
	< 25 (10 day average)	Harvey 1989
	< 25	North Carolina Code, 1991
Recreation	5	AWWA, 1990
Human Consumption	1 to 5*	North Carolina Code, 1992

*Up to 5 NTU are acceptable if the water supplier can demonstrate that the level of turbidity does not interfere with disinfection, maintenance of a disinfecting agent or microbiological determination.

Health Effects

The suspended particles that contribute to turbidity may be composed of organic and/or inorganic constituents. Because organic particulates may harbor pathogenic microorganisms, turbid conditions may increase the possibility of encountering a waterborne disease (USEPA, 1986; North Carolina Code, 1992).

Industrial Effects

Turbid water may not be suitable for use in industrial processes. An abundance of suspended solids may obstruct or scour pipes and machinery (Harvey, 1989).

Recreational Effects

Highly turbid waters may be hazardous to the welfare of swimmers and boaters. Turbidity may help to conceal potentially dangerous obstructions such as boulders and logs. Also, the organic constituents of turbid waters may harbor high concentrations of pathogenic bacteria, viruses, and protozoans (AWWA, 1990).

Environmental Effects

The array of turbidity-induced effects that can occur in a water body may change the composition of an aquatic community (Wilber, 1983). First, turbidity caused by a large volume of suspended sediment will reduce the extent to which light can penetrate the water column, thereby suppressing the photosynthetic activity of phytoplankton, algae, and macrophytes, especially those farther below the surface. If high turbidity is largely the result of high algal content, light penetration will be limited and primary production will, therefore, be restricted to

the uppermost strata of the water column. Cyanobacteria (blue-green algae) are favored in this situation because they possess flotation mechanisms which allow them to remain near the water's surface (McCabe and Sandretto, 1985). Excess turbidity leads to fewer photosynthetic organisms available to serve as food sources for many invertebrates. As a result, the overall numbers of invertebrates may decline, which may lead to a decline in the fish population (Wilber, 1983; McCabe and Sandretto, 1985).

If turbidity is largely due to excess nutrients, dissolved oxygen (DO) depletion may occur in the water body. The available excess nutrients will increase the rate at which microorganisms breakdown detritus, a process that requires DO. In addition, excess nutrients may result in increased algal growth. Although the algae's photosynthetic processes produce DO during the day, these algae also respire at night, a process that consumes DO. Large declines in fish communities are often the result of extensive DO depletion (Smith, 1990).

Sources

The sources of increased turbidity can either be point or non-point sources. Point sources of increased turbidity include sewage treatment plants. They may discharge organic particles during sewage bypass periods that directly contribute to turbidity. Also, sewage treatment plants may release dissolved nutrients in treated wastewater that may contribute to phytoplankton production, indirectly increasing turbidity. Non-point sources of increased turbidity may either be naturally occurring or anthropogenic. Naturally occurring non-point sources of turbidity include land-derived sand, silt, clay, and organic particles dislodged by rainfall and carried by overland flow. In addition, suspended organic matter may result from natural in-stream or in-lake detritus and particulate matter may be resuspended from the bottom sediments by changes in the speed or direction of the water current. Finally, phytoplankton production may be enhanced, thereby increasing turbidity, when nutrients are released from bottom sediments during seasonal turnovers and changes in water current. Anthropogenic non-point sources of increased turbidity include human activities, such as agriculture, that contribute sediment and nutrients to the water body and can substantially increase turbidity beyond natural levels (Straub, 1989).

Mode of Transport

Particulates can be carried by overland flow or resuspended from the substrate by changes in the speed or direction of the water current. Overland flow may also transport dissolved nutrients that contribute to phytoplankton growth.

Since 1993, remote sensing researchers have developed leading-edge procedures and algorithms to use airborne imaging spectrometers for measurement of turbidity and chlorophyll concentrations in Australian rivers and lakes, and for remote detection of the presence and extent of cyanobacterial blooms in other water bodies (Jupp et al., 1994). Synoptic views of chlorophyll, turbidity and presence of cyanobacteria are powerful tools for the nearly

instantaneous evaluation of river or lake dynamics, and may often be more cost-effective measurements of water quality than conventional ground-based water quality sampling. Techniques have also been developed which make it possible to map submerged coastal vegetation and mangroves with hyperspectral sensors (Dekker, 1997).

METHODS

Study Area

The study site is located in Southwest Ohio and includes the Great Miami River (a tributary of the Ohio river), as well as adjacent water bodies, including fishponds, reservoirs and other rivers that are tributaries of the Ohio River (Table 2).

The Great Miami River is situated in the Miami Basin, which encompasses the drainage basins of both the Little and Great Miami Rivers (Figures 1 and 2). The Miami basin includes most of southwestern Ohio and portions of Indiana. The major waterways are the Great Miami River (including the tributaries, the Stillwater and Mad Rivers), the Little Miami River, and Whitewater River in Indiana.

Landforms in the Great Miami River Watershed have been shaped by glaciations, which left flat-to-gently-rolling terrain, glacial till, and in some areas, exposed limestone and shale. Soils in the watershed tend to be neutral-to-slightly alkaline and drainage varies from well drained to very poorly drained, depending on parent material and topography. The river lies within a broad valley with a wide flood plain (Ohio EPA, 1997). The area drained by the major waterways includes both agricultural and urban lands (Ohio EPA, 1997). The Miami basin includes the major cities of Cincinnati and Dayton, Ohio, and the smaller cities of Hamilton and Middletown, Ohio along the Great Miami River. Currently, it is estimated that 70% of the total land area is used for agriculture, dominated by row crops of corn and soybeans. Urban areas occupy 13% of the land, forested areas occupying 7%, and wetlands and water bodies occupy 1% of the total land area in the Miami Basin (USGS, unpublished report).

The Ohio Environmental Protection Agency (Ohio EPA) noted that most industries and municipalities near the Great Miami River utilize groundwater as a principal water source but discharge treated wastewater to the river. Surface run off from agricultural or urban areas and industries along the river is not treated or impeded prior to entering the river (Ohio EPA, 1997). Both the U.S. Environmental Protection Agency (USEPA) and the U.S. Geological Survey (USGS) have identified six important water quality issues in the Miami basin. These include: 1) the degradation of surface-and ground-water quality by urban and agricultural sources of fertilizer and pesticides, 2) assessing the relative importance of point and non-point sources to contaminant loads in the Great and Little Miami River Basins, 3) habitat degradation and decreases in stream biodiversity as a result of urbanization, 4) the occurrence of water-borne pathogens in streams and shallow ground water in rural and urban land-use settings, 5) the effect of septic systems and combined sewer overflows on surface and shallow ground-water quality,

and 6) the disruption and fragmentation of stream habitats by low dams and impoundments and their effects on fish and benthic invertebrate communities (Ohio EPA, 1997).

Table 2: Status of data collected with the field parameters and their approximate geographic location, grouped by date. Numbers in brackets indicate sample size. Usually one data point represents an average of three replicates, particularly for chlorophyll and turbidity. The numbers represent: 1) Newton Fishpond sites; 2) Burnett Wood pond; 3) Little Miami River sewage treatment plant and Hannish Reservoir; 4) Licking River and 5) Great Miami River.

Parameter/ Date Collected	Preliminary Data			Pilot Data							
	1/26 - 3/4	3/2 4	4/1 2	5/ 1 4	6/ 9	7/2 3	8/ 6	9/ 8	9/ 9	9/2 8	9/3 0
In-vivo chlorophyll (53)		5	4	5	5	5	5				
Monochromatic chlorophyll (98)				5	5	5	5	5	5	5	5
Trichromatic chlorophyll (81)						5	5	5	5	5	5
Total Suspended Solids (TSS) (99)				5	5	5	5	5	5	5	5
Transect for TSS (57)								5	5	5	5
Turbidity (128)	1,2,3,4	5	4	5	5	5	5	5	5	5	5
Secchi disk depth (105)		5	4	5	5	5	5	5	5	5	5
Depth (56)								5	5	5	5
Temperature (77)					5	5	5	5	5	5	
Dissolved Oxygen (63)					5	5		5	5	5	
pH (69)						5	5	5	5	5	5
Water Chemistry ??								5	5	5	5
GPS data not differentially corrected (105)		5		5	5	5	5	5	5	5	5
GPS data with differential corrections (58)						5	5	5	5	5	5
Field spectrometer data (123)	1,2,3,4	5	4	5	5	5	5	5*	5	5	5
Absorption spectra data (40)					5	5		5	5	5	5
Light extinction coefficient from LiCor at surface (38)							5	5	5	5	5
Light extinction coefficient from field spectrometer underwater extension (7)								5			
Image								5	5		5



Figure 1: Location map of the Great Miami River within the Miami River Basin.

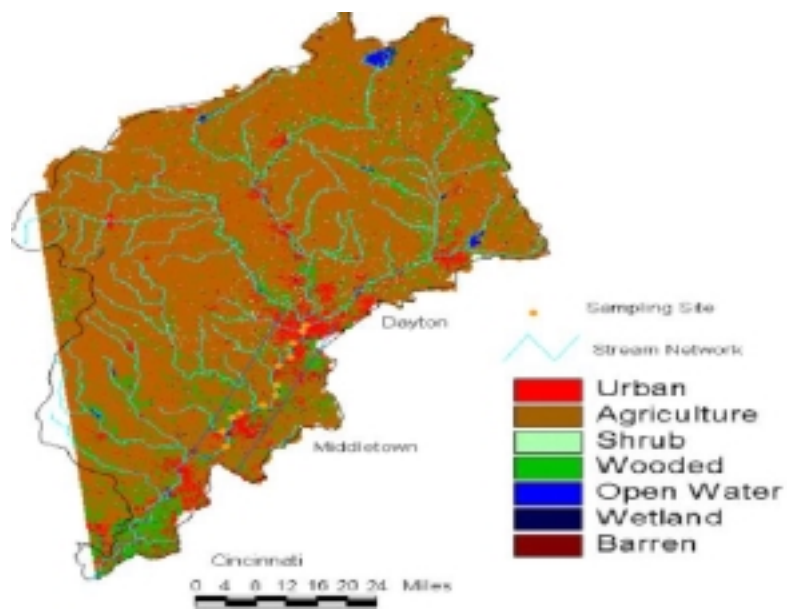


Figure 2: Sampling sites in the study area on the Great Miami River.

The presence of these environmental concerns in the Miami Basin and the availability of ancillary data in the offices of the USEPA, OEPA, Ohio Department of Natural Resources (ODNR), Natural Resources Conservation Commission (NRCS) and USGS make the Miami basin an appropriate pilot study site for this type of research. A map of the study locations within the Miami Basin is shown in Figure 2.

Data

Ground-truth (reference) and spectral data were collected from 26 January 1999 to 30 September 1999. The data can be roughly divided into two sets, preliminary and pilot, based on the date and location from which the data were collected and the amount of data collected. The preliminary data sets were collected from 26 January 1999 to 12 April 1999 and the pilot data sets were collected from 14 May 1999 to 30 September 1999. In addition, all pilot data were collected from the Great Miami River between river miles (RM) 45 and 92, where remote sensing imagery was acquired in the latter part of the study period. The purpose of the preliminary data was to examine the response of the Full Range Field Spectroradiometer (FieldSpec FR, Range 350-2,500 nm) to different water quality conditions found in the various water bodies. Generally, the preliminary spectral reading was accompanied by turbidity measurements using a field turbidimeter. In addition, in-vivo chlorophyll measurements were made on two additional dates. The pilot data are characterized by a more complete data set including in-vivo chlorophyll data (Table 2).

The other major data set for this project includes two sets of hyperspectral imagery. The two airborne sensors that acquired the imagery were the CASI, taken on 8 and 9 September 1999, and the Hyperspectral Mapping (HyMap), taken on 30 September 1999. The CASI acquired imagery in 19 spectral bands and the HyMap acquired imagery in 126 spectral bands.

Spectral Data Collection

Two types of spectral data were collected during the study period: above water reflectance spectra and underwater radiance or irradiance spectra. The reflectance data represent the ratio of reflected energy to incident energy with values ranging from 0.0 to 1.0. The irradiance data represent actual energy received by the sensor as downwelling (irradiance) or upwelling (radiance) in units of power per unit area per unit wavelength ($W/m^2/sr/nm$). The above water reflectance data were collected using the FieldSpec FR instrument from Analytical Spectra Devices (ASD), Inc., 1999. The underwater radiance spectra were collected using two methods. The first method used the FieldSpec FR instrument fitted with an underwater extension cord and an Underwater Remote Cosine Receptor (UWRCR). The second method used a Li-Cor brand light meter (LI-189) with an underwater sensor (LI-1000). While the FieldSpec FR samples energy (reflected or radiant) at 1-nm intervals, the Li-Cor measured an aggregate energy in the

visible range between 400 and 700 nm. Due to the amount of time it takes to assemble and disassemble the underwater extension to the FieldSpec FR, the underwater extension was used only during the first day of the CASI flyover (Table 2). Thus, the instrument of choice for most underwater light measurement was the Li-Cor meter (Table 2). An apparatus was constructed to position the sensors at the desired depth, pointing upward to measure downwelling irradiance and downward to measure upwelling radiance).

Imagery

CASI

On 8 and 9 September 1999, Hyperspectral Data International (HDI) flew the CASI sensor over the Great Miami River from approximately RM 45 to approximately RM 92. This sensor acquired data in 19 spectral bands with a spatial resolution of 2 m. Twenty three flightlines covered approximately 80 km (49.7 miles) of the Great Miami River, from Middletown, Ohio to the Taylorsville Dam, approximately 15 km (9.3 miles) north of Dayton, Ohio. The imagery was delivered on 36 compact discs (CDs) in a Band Sequential (BSQ) file format that was imported with the Environment for Visualizing Images (ENVI) processing software. Some of the flight lines were split into several segments for the purpose of pre-processing (HDI, 2000). Data obtained with the hand-held spectroradiometer were analyzed, revealing seven spectral bands that demonstrated usefulness for water quality studies. These include, bands 2 (440 nm), 7 (625 nm), 11 (672 nm), 14 (705 nm), 16 (740 nm), 17 (816 nm) and 18 (840 nm). These are the minimum number of bands that could be used to develop preliminary water quality maps.

HyMap

Analytical Imaging and Geophysics (AIG) acquired the HyMap data on 30 September 1999. As part of a collaborative program, AIG flew the HyMap sensor aboard an aircraft over the Great Miami River in the Dayton area for approximately 20 km (12.4 miles) from river length marker 112 km (69.6 RM) to river length marker 132 km (82.0 RM). This sensor collected data in 126 spectral bands with an average bandwidth of about 15 nm in the spectral range between 441 to 2478 nm. The reported nominal spatial resolution of the data was 5 m; however, the data were received with a resampled pixel size of 4 m (AIG, 1999). In addition, the data were received as raw data, without georeferencing. The geo-referencing procedures and files were included in the CD with the imagery. The imagery was atmospherically corrected for residual atmospheric and instrument effects utilizing the Atmospheric Removal Program (ATREM, Gao et al., 1996) and periodic noise was removed from the data using the EFFORT algorithm. Two adjacent flightlines were flown to cover the study area.

Table 3: Hyperspectral wavelength and band comparison of two Image dataset with hand-held Fieldspec FR dataset.

FieldSpec FR 350-2500 nm; 1nm interval		CASI 350-1000 nm; 5 nm interval		HyMap 440-2500 nm; 15 nm interval	
Band #	Wavelength (nm)	Band #	Wavelength (nm)	Band #	Wavelength (nm)
1	360	1	360		
2	370				
3	435				
4	440	2	440	1	441
5	455			2	458
6	460			3	472
7	482	3	482		
8	485				
9	490			4	488
				5	503
10	520			6	518
11	542	4	442	7	534
12	554	5	554	8	550
13	573	6	573	9	564
14	580			10	581
15	590			11	595
16	600				
17	610			12	610
18	620				
19	625	7	625	13	625
20	636	8	636		
21	648	9	648	14	642
22	656	10	656	15	656
23	672	11	672	16	671
24	675	12	675		
25	685			17	686
26	700	13	700		
27	702			18	703
28	705	14	705		
29	725	15	725	19	717
				20	732
30	740	16	740	21	747
				22	762
				23	778
				24	793
31	816	17	816	25	808
				26	823
32	840	18	840	27	838
				28	854
33	865	19	865	29	869
				30	884

To reduce the data size, only 40 bands were selected from the 126 bands. The 40 bands were in the range of 441 to 1043 nm. Because water strongly absorbs light in the near and mid-infrared regions, these bands cover the range where most of the information for water quality is contained. The selected bands of imagery were georeferenced using the HyMap georeferencing tool on ENVI software. An image mosaic was created using two georeferenced images (each representing a single flight line) to produce one scene containing both flight lines. To save disk space, only eight of the 40 bands in the original image were used in the mosaic. These eight bands were: b1 (441 nm), b2 (458 nm), b13 (625 nm), b16 (671 nm), b18 (703 nm), b19 (747 nm), b26 (823 nm) and b27 (838 nm). These bands were chosen based on their proximity to the bands selected in the CASI data sets and based on the results of the preliminary investigation using the hand-held sensor. In the lower wavelengths, band 1 is preferred, however, some pixels were shown to have unexpectedly high values for a water body and likely represented noise in the system. Therefore, band 2 is recommended as a substitute. Another option is to simply use band 1 and remove the outlying values from the analysis.

Criteria of Band Selection

Absorption

Through the components of light absorption and scattering coefficients, the water body controls the ratio between light scattering and absorption values, thus determining the subsurface reflectance and, in turn, the emergent flux that will be sensed by radiometers (Jupp et al., 1996). Because the medium composition affects the absorption and scattering coefficients differently at various wavelengths, the resulting spectral distribution can be mathematically modeled and/or measured by a spectroradiometer from above and under the water's surface, and thus can be used to provide information about the water body.

Both field and laboratory spectrometric measurements of reflectance and absorbance are essential to developing semi-empirical and analytical (radiative transfer) models that can describe the interactions of light and in-water materials (Dekker, 1997). Field spectrometry is the quantitative measurement of radiance, irradiance, reflectance or transmission of light in the field. There are many reasons why it is desirable to perform spectral measurements in the field. Field spectra of ground and water targets that are homogeneous at the scale of the imaging sensor and collected using ambient solar illumination can be used to convert radiance images to reflectance (Conel et al., 1987a,b). Often, field spectra of target materials are collected to allow for more precise image analysis and interpretation (Goetz and Srivastava, 1985). Hand-held spectroscopy is also used as a tool to perform feasibility studies to understand if and how a process or material of interest can be detected using remote sensing. Field spectra of both the material(s) of interest and spectra of other materials present in the environment can be used to address such issues as what spatial and spectral resolutions are required for detection. Lab spectroscopy measurements are also desirable because they are used for the determination of the

inherent optical properties of water by measuring the absorption and scattering spectra of dissolved materials and particulate matter.

Correlation

The correlation between temporally pooled ground-truth and spectral data was used to locate spectral signatures for water quality parameters. Replicate ground-truth data at a sampling point were averaged before conducting the correlation. Thus, when available, a data point represented the mean of three replicates. There were two spectral samples taken a few seconds apart at each sampling point. These values were averaged before calculating the correlation with the ground-truth data. A statistical summary of all ground-truth data was first computed using descriptive statistical parameters (e.g., mean, maximum value, minimum value). This allowed the data sets to be examined for the detection of the extreme outliers.

One of the tools used to quantify the relationship between the spectral data and the ground-truth data was a correlation matrix. Scatter plots of ground-truth data against spectral data and of ground-truth parameters of interest against each other were made to investigate relationship trends that may not be captured by correlation values. Depending on the magnitude of the correlation values and the trend in the scatter plots, linear and non-linear equations were developed to predict water quality parameters from spectral indices.

When direct relationships between spectral data and water quality parameters were not established due to lack of data or a weak relationship, an indirect approach was used with other co-varying parameters and the spectral data. For example, because algal biomass was not measured or collected, a literature-based equation (Algal biomass = Sample weight - Ash weight) was used to convert chlorophyll *a* concentrations ($\mu\text{g/l}$) into dry weight algal biomass (mg/l) (Millward, 1996). Similarly, due to a strong correlation between turbidity and TSS, a two-step procedure is recommended to estimate TSS levels from spectral data. First, turbidity will be estimated using spectral data, and then TSS can be estimated from those turbidity estimations.

First Derivative

Spectroscopic derivatives are tools that can be used in spectroscopy (Philpot, 1991). They are obtained by taking the difference between the reflectance of two bands and dividing that value by the difference between the wavelengths separating the two bands. Then, a correlation test is performed between derivative reflectance and the field measurement of turbidity. When the two bands used in the calculation are adjacent to one another, the result is the first derivative. It is assumed that the components of variation are additive constants acting in a spectrally-independent way over a spectral range of a few nanometers (nm). This assumption fits well with knowledge of the behavior of radiation and reflectance in the atmosphere and in water. Moreover, it is much less demanding than the assumption made for the use of broad waveband indices. The mathematical basis of derivative spectroscopy has been reviewed (Dixit and Ram,

1985) and applied to the remote sensing of vegetation (Curran, 1989; Demetriades-Shah et al., 1990; Curran et al., 1991).

The use of derivative spectroscopy for estimating turbidity and suspended particles are not frequently reported in the literature. However, its potential can be inferred from previous studies (Dick and Miller, 1991; Philpot, 1991) and demonstrated using three laboratory spectra (Chen et al., 1991). The derivative reflectance spectra vary in a regular way with turbidity. Regions of the spectrum at wavelengths near 450-550 nm, 675-750 nm and 800-1000 nm show particularly large changes in derivative reflectance with turbidity and these are, therefore, candidate spectral regions for the estimation of turbidity with derivative spectroscopy.

RESULTS AND DISCUSSION

The evaluation of band selection criteria lead to the selection of certain channels from the whole dataset for various water quality parameters (Table 4). The bands integral to the most significant parameters, chlorophyll *a* and turbidity, are discussed below.

Chlorophyll a

Chlorophyll *a* is a phytopigment present in all algae groups in inland waters and shows distinct absorption bands in the blue wavelength range at 440 nm and in the red wavelength range from 672-678 nm (Figure 3), leaving a maximum green reflectance due to an internal cell scattering process. The red edge ascent near 705 nm that is narrowed to a peak by growing water absorption in the infrared is also correlated to increasing chlorophyll *a* contents (Figure 4).

Based on the correlation with the ground-truth data, one of the most important relationships observed in this study was the relationship between turbidity, TSS, and chlorophyll. Turbidity was positively correlated with TSS ($r = 0.76$) and less positively correlated with chlorophyll ($r = 0.37$). Turbidity was negatively correlated with Secchi disk depth ($r = -0.55$), river depth ($r = -0.19$), and pH ($r = -0.64$). TSS was moderately correlated with chlorophyll parameters (up to $r = 0.51$). Of the chlorophyll parameters, turbidity and TSS generally appear to correlate better with a chlorophyll parameter that combines chlorophyll *a* and pheophytin data. Dissolved oxygen showed a low positive correlation ($r = 0$ to 0.49) with most parameters, but with a relatively stronger value with chlorophyll variables ($r = 0.44$), asserting that more living algal activity enriches the water with DO through the process of photosynthesis.

The two most significant bands, 672 nm and 705 nm, were selected for the calibration of chlorophyll *a* concentration. The ratio of 672 and 705 nm wave bands produced a good correlation ($r = 0.86$) with the chlorophyll *a* concentration (Figure 5). Using this linear model, a chlorophyll-*a* distribution map of the river was made (Figure 6). It is notable that a plume of water with a relatively low concentration of chlorophyll-*a* can be seen entering the river from a wastewater treatment plant (WWTP).

Table 4: Correlation values between spectral indices and water quality parameters that had the highest value in each group. Data were collected from January to September 1999.

Measurement	Indices			
	Individual Bands	Difference	Ratio	Combination
Turbidity	0.70 (702)	0.79 ¹	0.37 ⁴	0.80 ⁸
Secchi Depth	-0.25 (705)	-0.60 ²	-0.50 ⁵	0.69 ¹⁰
Depth	-0.35 (705)	-0.58 ¹	-0.47 ⁴	-0.61 ⁸
TSS	0.35 (705)	0.57 ³	-0.35 ⁶	-0.47 ¹⁰
In-vivo Chlorophyll	0.51 (490)	0.82 ³	0.86 ⁵	-0.89 ¹¹
Monochromatic Chlorophyll <i>a</i> (corrected)	-0.23 (656)	0.57 ³	0.59 ⁵	-0.73 ¹¹
Monochromatic Chlorophyll <i>a</i> (uncorrected)	-0.18 (656)	0.63 ³	0.64 ⁵	-0.77 ¹¹
PHA	-0.27 (672)	0.35 ³	0.53 ⁵	0.51 ¹²
Chlorophyll <i>a</i> (corrected)	-0.27 (672)	0.64 ³	0.71 ⁵	-0.79 ¹¹
Chlorophyll <i>a</i> (uncorrected)	-0.22 (672)	0.61 ³	0.68 ⁵	-0.74 ¹¹
Trichromatic Chlorophyll <i>a</i>	0.35 (705)	0.60 ³	-0.50 ⁶	-0.70 ¹¹
Trichromatic Chlorophyll <i>b</i>	0.18 (816)	0.21 ³	-0.32 ⁶	-0.33 ¹¹
Trichromatic Chlorophyll <i>c</i>	0.13 (816)	0.20 ³	-0.29 ⁶	-0.32 ¹¹
DO	0.38 (370)	0.18 ³	-0.49 ⁴	-0.22 ⁸
pH	-0.36 (636)	-0.61 ¹	0.25 ⁵	-0.58 ⁹
Temperature	-0.32 (370)	-0.29 ¹	-0.34 ⁷	0.33 ⁸
Light extinction coefficient (upwelling)	0.16 (816)	0.61 ³	0.53 ⁵	-0.70 ¹⁰
Light extinction coefficient (downwelling)	0.24 (816)	0.57 ³	0.44 ⁵	-0.67 ¹⁰

Difference Index: ¹(625 - 440), ²(702 - 672), ³(705 - 672)

Ratio Index: ⁴(625/440), ⁵(705/672), ⁶(702/740), ⁷(520/554)

Combination Index: ⁸(625 - 440)*(705/672), ⁹(625 - 440)*(685/672), ¹⁰(440 - 740)/(705-740), ¹¹(672 - 740)/(705 - 740), ¹²(705 - 672)/656

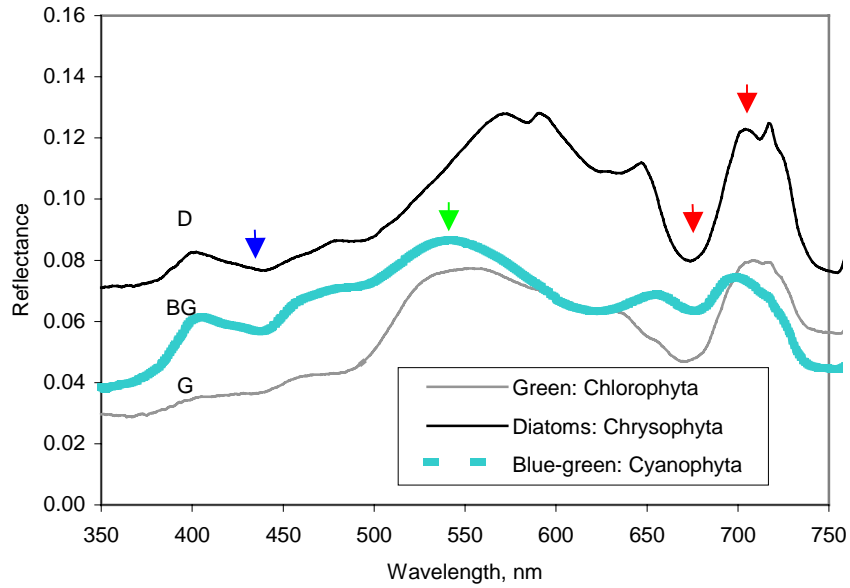


Figure 3: Maximum and minimum absorption values in the reflectance spectra of pure algal culture.

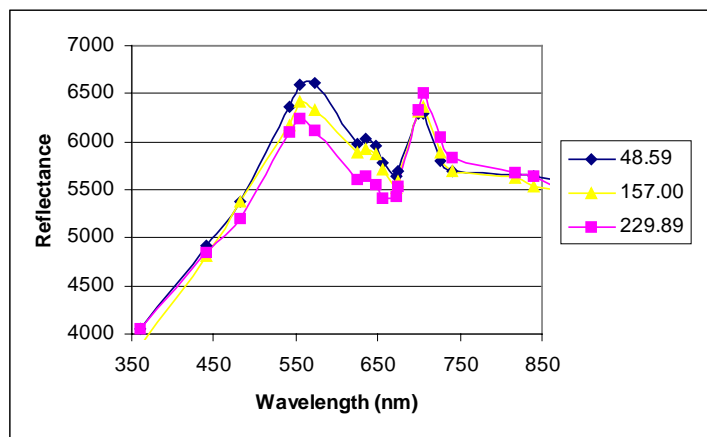


Figure 4: Reflectance spectra for known chlorophyll-a values from CASI data.

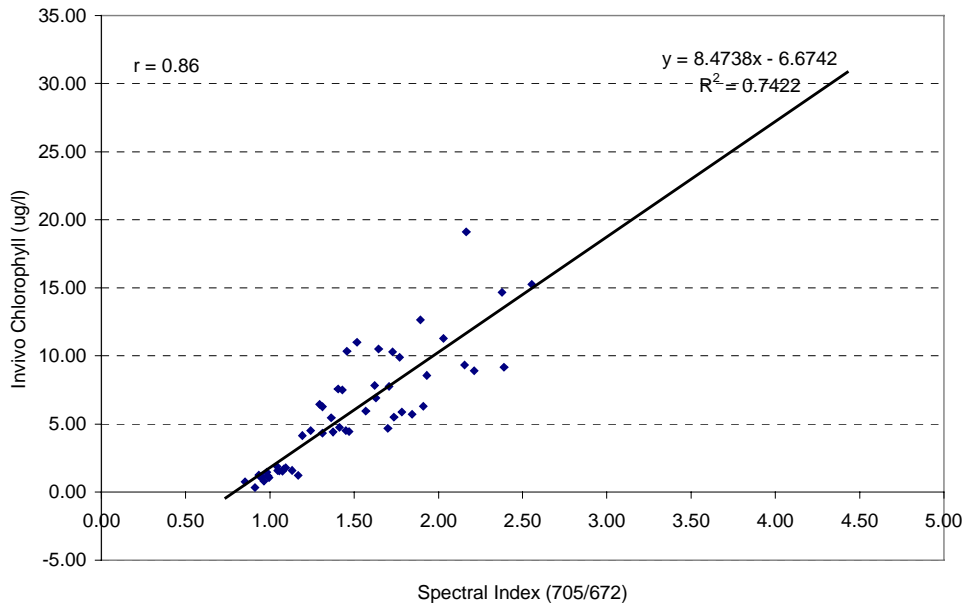


Figure 5: Correlation between spectral index and chlorophyll concentration obtained from ground truth data.

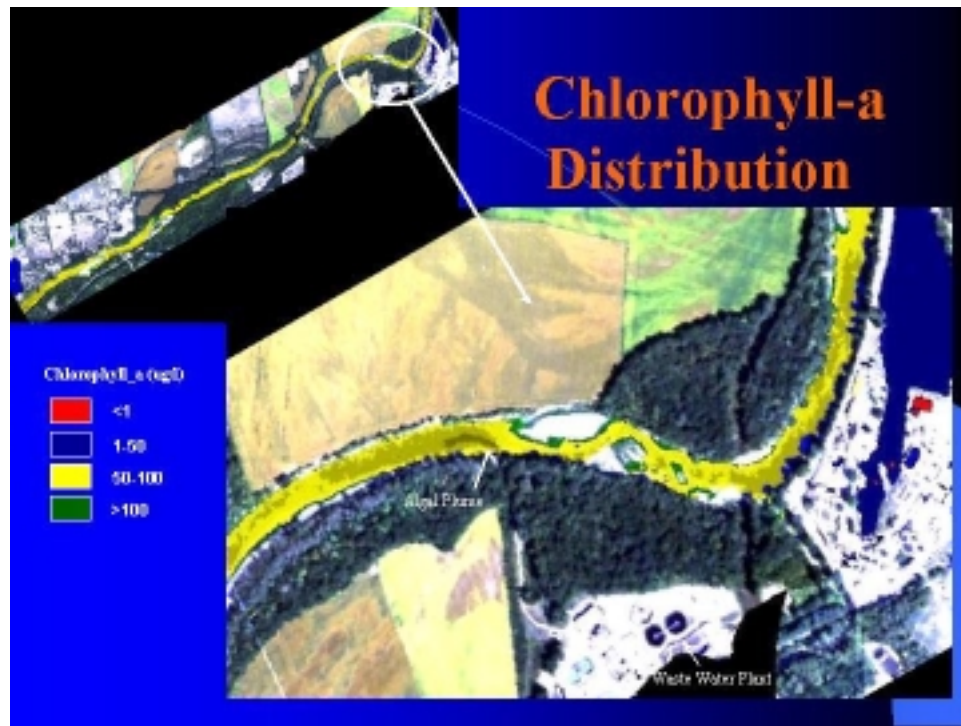


Figure 6: Chlorophyll-a concentration map developed from the spectral index.

Turbidity

To examine the association between spectral reflectance and turbidity, correlation analyses were applied to the Fieldspec FR channels between 400 and 880 nm. A strong relationship existed between turbidity and reflectance with $r = 0.8$ at $(625-440)*705/672$. However, this relationship resulted in much higher predicted values of turbidity in the river than the turbidity values that were actually collected on the ground. In an effort to improve results, first derivatives were calculated by dividing the difference between successive reflectivity values by the wavelength interval separating them. A correlogram for turbidity was developed using the first derivative and normal reflectance at a particular wavelength. Figure 7 illustrates the difference between the correlation coefficients from the raw reflectance data and the first derivative method.

The maximum correlation, $r = 0.76$ was found at the derivative of $(700-675)/25$ nm (Figure 7). Therefore, the bands at this wavelength were selected for the turbidity measurement.

The first derivative reflectance and turbidity scatter plot (Figure 8) fits with a linear model:

$$\text{Turbidity} = 1224.4 * (R(685)) + 3.9561 \quad \text{with } R^2 = 0.7917$$

Using this linear model, a turbidity map of the river was made (Figure 9). This model showed a strong agreement between observed and estimated turbidity values (Figure 10).

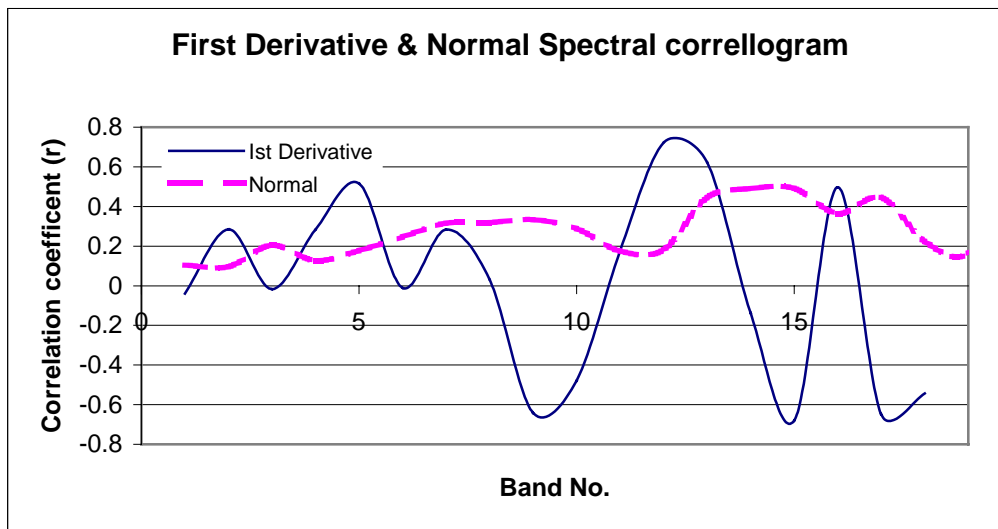


Figure 7: Comparison between first derivative and normal correlogram. A higher correlation is obtained from the first derivative.

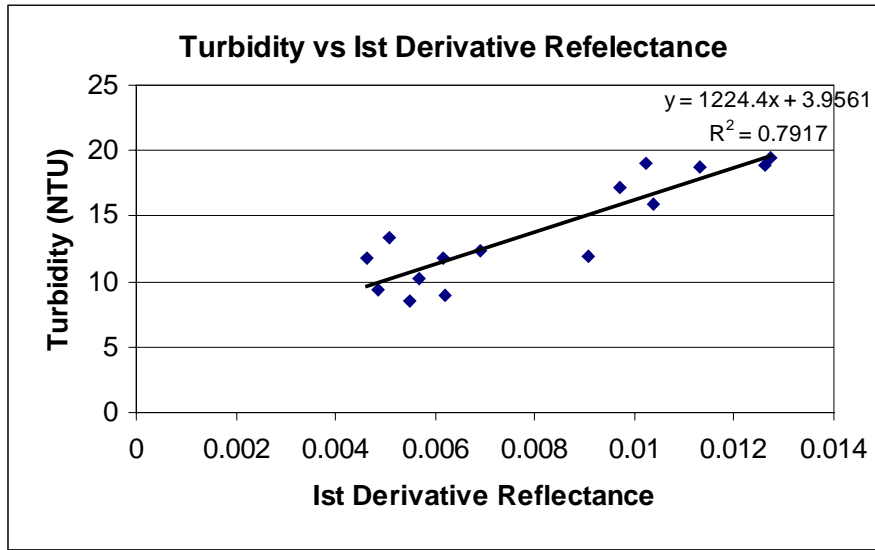


Figure 8: Correlation between first derivative reflectance and turbidity, obtained from the Fieldspec FR data

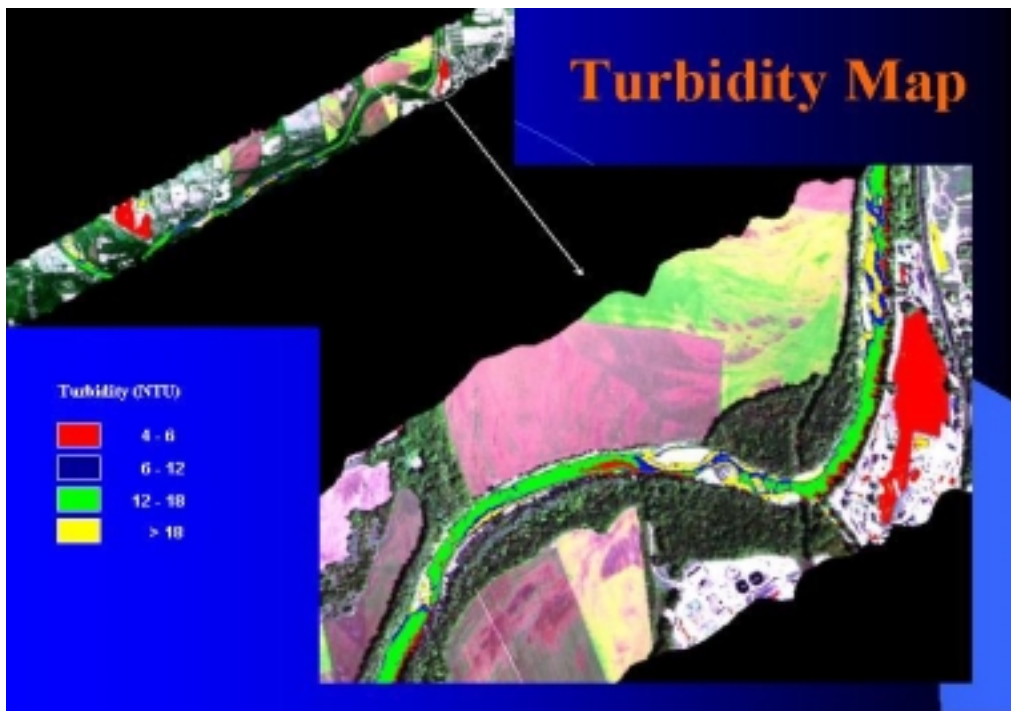


Figure 9: Turbidity distribution map of GMR, relatively clear water is entering into the river from the WWTP

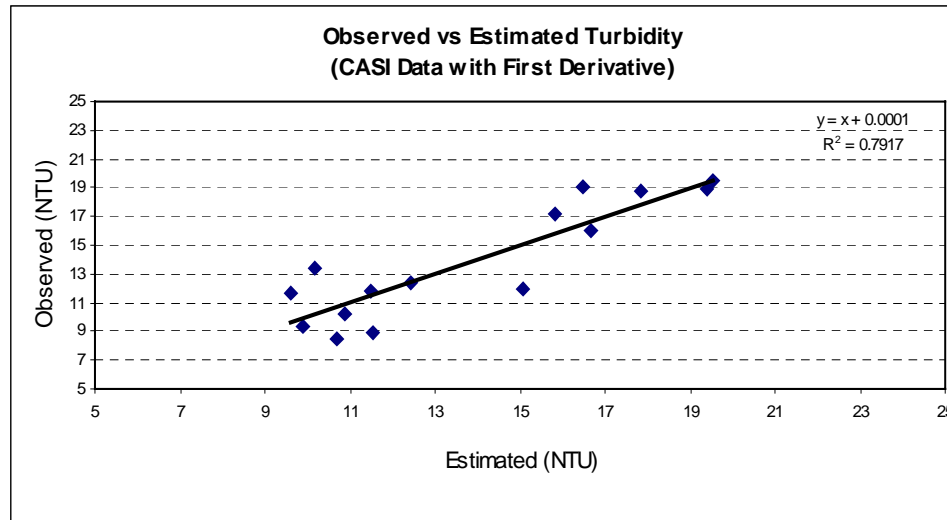


Figure 10: Observed and estimated turbidity plot.

CONCLUSIONS

Remotely sensed hyperspectral data have been used successfully to map the spatial distribution of chlorophyll-*a* concentrations and turbidity in the Great Miami River, Ohio. Spectral signatures from the hand-held spectrometer and airborne hyperspectral imagery showed promising correlations with ground-truth water quality parameters such as algal chlorophyll concentrations, turbidity values, Secchi disk depths and light extinction coefficients. Due to the presence of the strong correlation between laboratory-measured TSS and derivative reflectance with both field spectrometer data and CASI data, a first derivative spectrometry was used which showed promising results for the low-turbidity conditions of the Great Miami River. This was not possible with normal (i.e., ratio or combination) indices due to the lack of gradient in actual turbidity measurements. The uniformity in the distribution of turbidity for most of the river was confirmed by the imagery and the final map. Finally, maps of relative spatial distributions of chlorophyll and turbidity were created from the selected signatures derived from the imaging spectrometer data.

The hyperspectral chlorophyll and turbidity map demonstrate the spatial variability of the contents of chlorophyll and suspended matter that help determining the point and non point sources responsible for the spatial variability in eutrophic indicators in the Great Miami River. As a result, these maps may help resource managers locate monitoring locations that are more representative of the river's levels of suspended matter and related parameters such as chlorophyll and Secchi depth. Overall, this study shows that the combined use of traditional water quality monitoring with remotely sensed and in-situ hyperspectral data aided in the broad-scale characterization of the Great Miami River. With further development, these methods can be used to characterize the eutrophic conditions on other rivers.

REFERENCES

- Analytical Imaging and Geophysics (AIG). 1999.
(http://www.aigllc.com/data_acq/hymap_199/hym_tut1.htm)
- American Water Works Association (AWWA). 1990. Water Quality and Treatment, 4th edition, F.W. Pontius (technical ed.), McGraw-Hill, Inc., New York, NY.
- Chen, Z., J.D. Hanson, and P.J. Curran. 1991. The form of the relationship between suspended sediment concentration and spectral reflectance and its implications for the use of Daedalus 1268 data, *Int. J. Remote Sens.*, 12:15-222.
- Conel J.E., C.J. Bruegge, and B. Curtiss. 1987a. Correcting airborne imaging spectrometer measurements for the atmosphere: A comparison of methods. Proc. 31st. S.P.I.E. International Technical Symposium on Optical and Optoelectronic Applied Science and Engineering.
- Conel J.E., R.O. Green, G. Vane, C.J. Bruegge, R.E. Alley, and B. Curtiss. 1987b. AIS-2 Radiometry and a comparison of methods for the recovery of ground reflectance. Proc. 3rd Airborne Imaging Spectrometer Data Analysis Workshop.
- Curran, P.J. 1989. Remote sensing of foliar chemistry, *Remote Sens. Environ.* 29:271-278.
- Curran, P.J., J.L. Dungan, B.A. Macler, and S.E. Plumer. 1991. The effect of a red leaf pigment on the relationship between red edge and chlorophyll concentration, *Remote Sens. Environ.* 35:69-76.
- Dekker, A.G. 1997. Operational tools for remote sensing of water quality: A prototype tool kit. Vrije Universiteit, Amsterdam Institute for Environmental Studies. BCRS Report 96-18, ISBN 90 5411 215 8.
- Demetriades-Shah, T.H., M.D. Steven, and J.A. Clark. 1990. High resolution derivative spectra in remote sensing, *Remote Sense. Environ.* 33:55-64.
- Dick, K., and J. Miller. 1991. Derivative analysis applied to high resolution optical spectra of freshwater lakes. Proc. 14th Canadian Symposium on Remote Sensing, Canadian Remote Sensing Society, Ottawa, pp. 400-418.
- Dixit, L. and S. Ram. 1985. Quantitative analysis by derivative electronic spectroscopy, *Appl. Spectrosc. Rev.* 21:311-418.
- Gao, B.C., K.B. Heidebrecht, and A.F.H. Goetz. 1996. Atmospheric Removal Program (ATREM) user's guide. Centre for the Study of Earth from Space, Cooperative Institute for Research in Environmental Science, University of Colorado, Bolder.

- Goetz, A.F.H. and V. Srivastava. 1985. Mineralogical mapping in the Cuprite mining district, Nevada, Proc. Airborne Imaging Spectrometer Data Analysis Workshop, April 1985, JPL Publication, no. 85-41.
- Harding, L.W., E.C. Itsweire, and W.E. Esalas. 1995. Algorithm development for recovering chlorophyll concentrations in the Chesapeake Bay using aircraft remote sensing, 1989-91. *Photogrammetric Engineering & Remote Sensing*, 61(2):177-185.
- Harvey, G.W. 1989. Technical review of sediment criteria, for consideration for inclusion in Idaho Water Quality Standards. Idaho Dept. of Health and Welfare, Water Quality Bureau, Boise, ID.
- Hyperspectral Data International (HDI), Inc. 2000. Final Report: Great Miami River Remote Sensing Project. Work Number 99RD037R. Hyperspectral Data International, Inc., Dartmouth, Nova Scotia, Canada. 57 pp.
- Jupp, D.L.B., J.T.O Kirk, and G.P. Harris. 1994. Detection, identification and mapping of cyanobacteria: Using remote sensing to measure the optical water quality of turbid inland waters, *Aust. J. Mar. Freshwater Res.*, 45:801-28.
- Kuo, J.T., J.H. Wu, and W.S. Chu. 1994. Water quality simulation of Te-Chi Reservoir using two-dimensional models. *Wat. Sci. Tech* 30(2):63-72.
- Kuo, J.T., and J.H. Wu. 1991. A nutrient model for a lake with time-variable volumes. *Wat. Sci. Tech* 24(6):133-139.
- Lathrop, R.G., and T.M. Lillesand. 1989. Monitoring water quality and river plume transport in Green Bay, Lake Michigan with SPOT-1 imagery. *Photogrammetric Engineering & Remote Sensing*, 55(3):349- 354.
- Lillesand, T.M., W.L. Johnson, R.L. Deuell, O.M. Lindstrom, and D.E. Meisner. 1983. Use of Landsat data to predict the trophic state of Minnesota Lakes. *Photogrammetric Engineering & Remote Sensing*, 49(2):219-229.
- Lung, W.S. 1986. Assessing phosphorus control in the James River Basin. *Journal of Environmental Engineering*, 112(1):44-60.
- McCabe, J.M., and C.L. Sandretto. 1985. Some aquatic impacts of sediment, nutrients, and pesticides in agricultural runoff. Limnological Research Laboratory, Dept. of Fisheries and Wildlife, Michigan State University. Publication No. 201.
- Millward, M.R. 1996. Utilization of detrital food by Ohio River zebra mussels. Master's Thesis. University of Cincinnati, Cincinnati, OH.

North Carolina Administrative Code Section 15A.NCAC.2B-.0200. 1991. Classifications and water quality standards applicable to surface waters of North Carolina. North Carolina Department of Environment, Health and Natural Resources, Division of Environmental Management, Raleigh, N.C.

North Carolina Administrative Code Section T15A.18C.0101-.0102. 1992. Rules governing public water systems. North Carolina Department of Environment, Health, and Natural Resources, Division of Environmental Health, Raleigh, N.C.

Ohio EPA. 1997. Biological and water quality study of the Middle to Lower Great Miami River and Selected tributaries. Division of Surface Waters, Monitoring and Assessment Section, Columbus, OH. Ohio EPA Technical Report MAS/1996-12-8.

Philpot, W.D. 1991. The derivative ratio algorithm: Avoiding atmospheric effects in remote sensing, *IEEE Trans. Geosci. Remote Sens.* 29:250-357.

Ritchie, J.C., and C.M. Cooper. 1991. An algorithm for estimation surface suspended sediment concentrations with Landsat MSS digital data, *Water Resources Bulletin*, 27(3):373-379.

Ruiz-Azuara, P. 1995. Multitemporal analysis of "simultaneous" Landsat imagery (MSS and TM) for monitoring primary production in a small tropical coastal lagoon, *Photogrammetric Engineering & Remote Sensing*, 61(2):877-198.

Smith, R.L. 1990. Ecology and field biology. 4th ed. Harper Collins, New York, NY.

Straub, C.P. 1989. Practical handbook of environmental control. CRC Press, Inc., Boca Raton, FL.